INT. J. NUM. METH. HEAT FLUID FLOW, VOL. 6, NO. 8, 53–70 (1996)

NUMERICAL STUDY OF THE EARLY STAGES OF IMPULSIVELY STARTED UNSTEADY LAMINAR FLOW PAST A SQUARE CYLINDER

T.S. LEE, R.S.TAN AND X.P. XU

Mechanical and Production Engineering Department, National University of Singapore, Singapore

ABSTRACT

The time development of the symmetrical standing zones of recirculation, which is formed in the early stages of the impulsively started laminar flow over the square cylinder, have been studied numerically. The Reynolds number considered ranges from 25 to 1,000. Main flow characteristics of the developing recirculation region aft of the square cylinder and its interaction with the separating shear layer from the leading edges are studied through the developing streamlines. Other flow characteristics are analysed in terms of pressure contours, surface pressure coefficient, wake length and drag coefficient. Four main-flow types and three subflow types of regimes are identified through a detailed analysis of the evolution of the flow characteristics. Typically, for a given Reynolds number, it is noted that flow starts with no separation (type I main-flow). As time advances, symmetrical standing zone of recirculation develops aft of the square cylinder (type II main-flow). The rate of growth in width, length and structure of the aft end eddies (sub-flow (a)) depends on the Reynolds number. In time, separated flow from the leading edges of the square cylinder also develops (type III main-flow) and forms growing separation bubbles (sub-flow (b)) on the upper and lower surfaces of the square cylinder. As time advances, the separation bubbles on the upper and lower surfaces of the cylinder grow towards downstream regions and eventually merge with the swelling symmetrical eddies aft of the cylinder. This merging of the type II and type III flows created a complex type IV main-flow regime with a disturbed tertiary flow zone (sub-flow (c)) near the merging junction. Eventually, depending on the Reynolds number, the flow develops into a particular category of symmetrical standing recirculatory flow of specific characteristics.

KEY WORDS Early stages Impulsively started flow Square cylinders

INTRODUCTION

Separated flow over bluff bodies such as circular cylinders, square cylinders, rectangular cylinders and flat plates has been investigated by various researchers. Davis and Moore[1] studied vortex shedding from two-dimensional time-dependent flow past rectangular cylinders. They noted that due to the build-up of fluid in the recirculation zones behind the body prior to the initiation of shedding, the initial vortices that came off were very large followed by some smaller and regularly shaped vortices that appeared once steady-state shedding was reached. Nagano[2] investigated similar flow over a rectangular cylinder by the discrete vortex model instead of solving the Navier-Stokes equations by finite difference or finite element method. Fernando and Modi[3] used a more sophisticated numerical approach – the boundary element method in conjunction with the discrete vortex model – to represent the complex unsteady flow field around a bluff body with separating shear layers. Lisa and Balasubramaniam[4] used a finite element method to investigate the Strouhal frequencies in vortex shedding over square cylinders with

0961–5539/96

Received March 1996

surface suction and blowing. Kim and Benson[5] made a comparison of various numerical methods: the SMAC, PISO and iterative time advancing schemes for unsteady flows past a circular and a square cylinder. The capability of each scheme to solve the unsteady flows was found to be attributed to a pressure correction algorithm that strongly enforced the conservation of mass. For experimental work, many researchers studied the low Reynolds number flow around circular, rectangular and square cylinders. Bearman and Trueman[6] carried out a flow visualization study of flow over rectangular cylinders. They showed that the drag coefficient was found to be strongly influenced by the presence of the trailing corners. Coutanceau and Bouard[7] and Bouard and Coutanceau[8] used flow visualization as their main tool for studying the wakes behind an impulsively started flow past circular cylinders. They were interested in the near wake evaluation. They found that the characteristics of the pair of symmetric standing eddies and the appearance of secondary phenomena near the wake region depend on the initial Reynolds number. The characteristics of the early wake development can have a strong influence on the evaluation of effects of secondary phenomena. Gerrard[9,10] carried out a series of experiments providing very careful flow visualization studies on a circular cylinder in water using a towing tank. At a certain Reynolds number, the length of the recirculation region containing a pair of contra-rotating standing eddies was found to be approximately two cylinder diameters long. At higher Reynolds numbers, Gerrard observed dye which had rolled up into a vortex returning towards the cylinder in what he referred to as a "finger". Gerrard[10] also observed the three-dimensional nature of the wake flow, as time progressed from the initial start-up of the motion, the influence of the ends began to spread across the span and gave rise to bowed vortices. Okajima[11] and Okajima and Kitajima[12] investigated the fluid behaviour around square and rectangular cylinders in a wind tunnel and in a water tank. For the cylinders with width to height ratios of 2 and 3, there existed a certain range of Reynolds numbers where the abrupt change of flow pattern occurred with a sudden discontinuity in the Strouhal-number curves. For the Reynolds number below that region, the flow separated at the leading edges reattached on either the upper or the lower surface during a period of vortex shedding. For Reynolds numbers beyond it, the flow tended to reattach on the cylinder owing to the increasing effects of the Reynolds stressed and turbulent entertainment at a high Reynolds number. More recently, Kyoji and Yoshifumi[13] visualized water flows over a circular cylinder and a trapezoidal cylinder in a circular pipe in order to investigate the complexity of the flow in a flowmeter. From their experiment, it was shown that the formation of Karman-vortex-like vortices are three-dimensional in nature when forming behind a circular cylinder or a trapezoidal cylinder as the separated shear layer wrapped up the fluid just behind the cylinder. Also, the leading edge of the separation region was observed to move up to a certain distance behind the circular cylinder with the increasing Reynolds number.

The above studies of flow over circular, rectangular and square cylinders are of direct relevance to many engineering applications such as the design of flow meters, designs of tower structures, suspension bridges, chimneys, heat exchangers, road vehicles, tall buildings, etc. Most of the above work focused on long-term flow development. Few considered the use of numerical methods in their studies for the impulsively started flow. This is because of the complexity and numerical accuracy required for the impulsively started fluid flow problems. However, the evolution of the separated flow around cylinders at the early stages is known to have a strong influence on the long-term wake development. Hence, detailed study of the flow development characteristics of well defined separation flows are necessary for the understanding of the building up of the recirculation zone before they are burst into smaller Karman-type vortices. In the present study, the flow-governing equations are expressed in generalized curvilinear co-ordinate system. This allows the implementation of a numerical scheme on the Cartesian grid where the geometric characters are embedded in the coefficients of the transformed equations. The equations for any two-dimensional cross-sections are then obtained by specifying suitable coefficients for the transformed governing equations. All the transported properties are expressed in their conservative form.

GOVERNING EQUATIONS AND NUMERICAL PROCEDURE

The solution domain of the impulsively started flow past a square cylinder is shown in Figure 1. The square cylinder is placed slightly forward along the axis of symmetry in the solution domain. The two-dimensional governing equations, expressed in a generalized curvilinear co-ordinate system, describing the flow over the square cylinder at any instant of time, are given by

$$\frac{\partial U}{\partial \xi}+\frac{\partial V}{\partial \eta}=0 \tag{1}$$

$$J\frac{\partial u}{\partial t}+\frac{J}{R_e}\frac{\partial(uU+p\xi_x)}{\partial \xi}+\frac{J}{R_e}\frac{\partial(uV+p\eta_x)}{\partial \eta}=\frac{J}{R_e}\frac{\partial(g^{11}u_\xi+g^{12}u_\eta)}{\partial \xi}+\frac{J}{R_e}\frac{\partial(g^{21}u_\xi+g^{22}u_\eta)}{\partial \eta} \tag{2}$$

$$J\frac{\partial v}{\partial t}+\frac{J}{R_e}\frac{\partial(vU+p\xi_y)}{\partial \xi}+\frac{J}{R_e}\frac{\partial(vV+p\eta_y)}{\partial \eta}=\frac{J}{R_e}\frac{\partial(g^{11}v_\xi+g^{12}v_\eta)}{\partial \xi}+\frac{J}{R_e}\frac{\partial(g^{21}v_\xi+g^{22}v_\eta)}{\partial \eta} \tag{3}$$

with $\mathrm{Re}=\rho u_0 L/\mu$. The non-dimensional variables are defined as:

$$u=\frac{\bar{u}}{u_0} \qquad v=\frac{\bar{v}}{v_0} \qquad p=\frac{\bar{p}}{\rho u_0^{\,2}} \qquad x=\frac{\bar{x}}{L} \qquad y=\frac{\bar{y}}{L} \qquad t=\frac{\bar{t}}{T_0}$$

where u_0 and L are references quantities and the over-bar denotes a dimensional parameter. In this study, u_0 equals u_∞, $L = d$ is the dimension of the side of the square cylinder, $T_0 = L/u_0$ may be interpreted as the time required for the impulsively started flow to move over one square spacing. Thus, t is equivalent to the number of square spacings the flow has moved since its impulsive start.

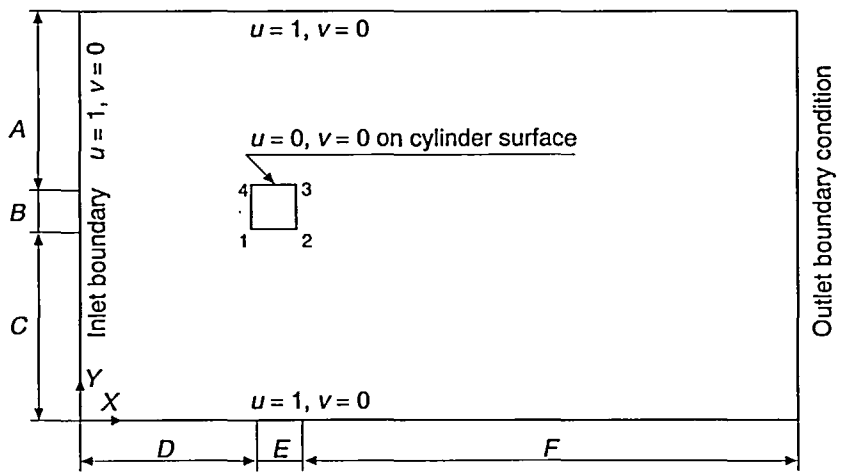

Figure 1 Problem definition of flow past a square cylinder

The curvilinear velocity U, V and the Cartesian velocity components u, v are related by

$$U = u\xi_x + v\xi_y, \quad V = u\eta_x + v\eta_y \tag{4}$$

The Jacobian matrix J and the matrix terms ξ_x, ξ_y, η_x, η_y are obtained from

$$\xi_x = \frac{y_\eta}{J}, \quad \xi_y = -\frac{x_\eta}{J}, \quad \eta_x = -\frac{y_\xi}{J}, \quad \eta_y = \frac{x_\xi}{J} \tag{5}$$

and the tensor components g^{11}, g^{12}, g^{21} and g^{22} are represented by

$$g^{11} = \xi_x^2 + \xi_y^2 \qquad g^{12} = \xi_x\eta_x + \xi_y\eta_y \qquad g^{21} = g^{12} \qquad g^{22} = \eta_x^2 + \eta_y^2 \tag{6}$$

Boundary conditions around the computational domain are defined as follows. At the inlet boundary, a uniform velocity distribution is assumed. The Neumann condition that the normal derivative equals zero is made at the outlet boundary. Along the other two horizontal boundaries, the flows are assumed to be sufficiently far from the influence by the presence of the square cylinder. Hence, the horizontal velocity component is assumed to be the undisturbed uniform velocity value and the normal velocity component is assumed to be zero. Non-slip conditions are prescribed at the surfaces of the square cylinder.

With the defined boundary conditions, equations (1)-(3) are solved by an iterative process, and all the physical variables (velocities and pressure) are updated as:

$$u_\xi^{n+1} = u_\xi^n + \delta u_\xi, \qquad u_\eta^{n+1} = u_\eta^n + \delta u_\eta, \qquad p^{n+1} = p^n + \delta p \tag{7}$$

where n and (n + 1) are previous and current iterative levels respectively. Substituting equation (7) into equations (1)-(3), and neglecting the second-order incremental terms, the governing equations are expressed in incremental variables form as:

$$\frac{\partial \delta U}{\partial \xi} + \frac{\partial \delta V}{\partial \eta} = -R_c \tag{8}$$

where

$$J\frac{\partial u}{\partial t} + \frac{J}{R_e}\frac{\partial \delta(uU + p\xi_x)}{\partial \xi} + \frac{J}{R_e}\frac{\partial \delta(uV + p\eta_x)}{\partial \eta} - \frac{J}{R_e}\frac{\partial \delta(g^{11}u_\xi + g^{12}u_\eta)}{\partial \xi} - \frac{J}{R_e}\frac{\partial \delta(g^{21}u_\xi + g^{22}u_\eta)}{\partial \eta} = R_\xi \tag{9}$$

$$J\frac{\partial v}{\partial t} + \frac{J}{R_e}\frac{\partial \delta(vU + p\xi_y)}{\partial \xi} + \frac{J}{R_e}\frac{\partial \delta(vV + p\eta_y)}{\partial \eta} - \frac{J}{R_e}\frac{\partial \delta(g^{11}v_\xi + g^{12}v_\eta)}{\partial \xi} - \frac{J}{R_e}\frac{\partial \delta(g^{21}v_\xi + g^{22}v_\eta)}{\partial \eta} = R_\eta \tag{10}$$

where

$$R_c = \frac{\partial U^n}{\partial \xi} + \frac{\partial V^n}{\partial \eta}$$

$$R_\xi = \frac{J}{R_e}\frac{\partial (uU + p\xi_x)^n}{\partial \xi} + \frac{J}{R_e}\frac{\partial (uV + p\eta_x)^n}{\partial \eta} - \frac{J}{R_e}\frac{\partial (g^{11}u_\xi + g^{12}u_\eta)^n}{\partial \xi} - \frac{J}{R_e}\frac{\partial (g^{21}u_\xi + g^{22}u_\eta)^n}{\partial \eta}$$

$$R_\eta = \frac{J}{R_e}\frac{\partial (vU + p\xi_y)^n}{\partial \xi} + \frac{J}{R_e}\frac{\partial (vV + p\eta_y)^n}{\partial \eta} - \frac{J}{R_e}\frac{\partial (g^{11}v_\xi + g^{12}v_\eta)^n}{\partial \xi} - \frac{J}{R_e}\frac{\partial (g^{21}v_\xi + g^{22}v_\eta)^n}{\partial \eta}$$

The R_c, R_ξ and R_η represent, respectively, the residuals of the continuity equation and two momentum equations at the nth iterative level. A procedure similar to the SIMPLE algorithm[14] is

chosen to solve equations (8)-(10) on a non-staggered grid. The difference schemes implemented for the various incremental terms are: the hybrid scheme for the convection-related terms; the central scheme for the diffusion terms; the first-order forward scheme for pressure terms and the backward difference schemes for the continuity equation. These are outlined below.

$$\frac{\partial\phi}{\partial r}=\frac{\phi_{i+1}-\phi_{i-1}}{2\Delta r}\omega+\frac{\phi_i-\phi_{i-1}}{\Delta r}(1-\omega)A+\frac{\phi_{i+1}-\phi_i}{\Delta r}(1-\omega)B$$

where $\phi=\delta u_\xi, \delta u_\eta$ are used for convection related terms, r is ξ or η and i is the index of grid point. The parameters ω, A and B are determined by the local cell Reynolds number (Rel) as follows:

if $|Rel| < 2.0$, then $\omega = 1.0, A = 0.0, B = 0.0$

if $|Rel| \le 2.0$, then $\omega = 1.0, A = 1.0, B = 0.0$

if $|Rel| \ge 2.0$, then $\omega = 0.0, A = 0.0, B = 1.0$

where $Rel = u_\xi \cdot \Delta\xi \cdot Re$ or $u_\eta \cdot \Delta\eta \cdot Re$ for the convective terms in ξ- or η-direction respectively.

$$\frac{\partial^2\delta\phi}{\partial\xi^2}=\frac{\delta\phi_{i+1,j}-2\delta\phi_{i,j}+\delta\phi_{i-1,j}}{\Delta\xi^2},\qquad \frac{\partial^2\delta\phi}{\partial\eta^2}=\frac{\delta\phi_{i,j+1}-2\delta\phi_{i,j}+\delta\phi_{i,j-1}}{\Delta\eta^2}$$

are used for the diffusion terms.

$$\frac{\partial\delta\phi}{\partial\xi}=\frac{\delta\phi_{i,j}-\delta\phi_{i-1,j}}{\Delta\xi},\quad \frac{\partial\delta\phi}{\partial\eta}=\frac{\delta\phi_{i,j}-\delta\phi_{i,j-1}}{\Delta\eta}\qquad \text{for the continuity equations}$$

and $$\frac{\partial\delta p}{\partial\xi}=\frac{\delta p_{i+1,j}-\delta p_{i,j}}{\Delta\xi},\quad \frac{\partial\delta p}{\partial\eta}=\frac{\delta p_{i,j+1}-\delta p_{i,j}}{\Delta\eta}\qquad \text{for pressure terms.}$$

The residuals are calculated by using the consistent second-order schemes. The second-order upwind schemes are used for the convection terms, the three-point central difference schemes for diffusive terms, the second-order forward schemes for the pressure terms and the second-order backward schemes for the continuity equations. At the grid points adjacent to the boundary, the central difference schemes are used for each variable. The details are described as follows.

The convection terms are discretized as:

$$u_\xi\frac{\partial\phi}{\partial\xi}=\begin{cases}u_{\xi i,j}\dfrac{3\phi_{i,j}-4\phi_{i-1,j}+\phi_{i-2,j}}{2\Delta\xi} & if\ u_{\xi i,j}\ge 0\\ u_{\xi i,j}\dfrac{-3\phi_{i,j}+4\phi_{i+1,j}-\phi_{i+2,j}}{2\Delta\xi} & if\ u_{\xi i,j}<0\end{cases}\qquad \text{for inner points}$$

$$u_\eta\frac{\partial\phi}{\partial\eta}=\begin{cases}u_{\eta i,j}\dfrac{3\phi_{i,j}-4\phi_{i,j-1}+\phi_{i,j-2}}{2\Delta\eta} & if\ u_{\eta i,j}\ge 0\\ u_{\eta i,j}\dfrac{-3\phi_{i,j}+4\phi_{i,j+1}-\phi_{i,j+2}}{2\Delta\eta} & if\ u_{\eta i,j}<0\end{cases}\qquad \text{for inner points}$$

and $$u_\xi\frac{\partial\phi}{\partial\xi}=u_{\xi i,j}\frac{\phi_{i+1,j}-\phi_{i-1,j}}{2\Delta\xi},\quad u_\eta\frac{\partial\phi}{\partial\eta}=u_{\eta i,j}\frac{\phi_{i,j+1}-\phi_{i,j-1}}{2\Delta\eta}$$

for points adjacent to boundary.

The diffusion terms are discretized in the same way as the incremental diffusion terms. The second-order forward schemes for pressure terms are:

$$\frac{\partial p}{\partial \xi}=\frac{-3p_{i,j}+4p_{i+1,j}-p_{i+2,j}}{2\Delta\xi},\quad \frac{\partial p}{\partial \eta}=\frac{-3p_{i,j}+4p_{i,j+1}-p_{i,j+2}}{2\Delta\eta}\quad \text{for inner points}$$

$$\frac{\partial p}{\partial \xi}=\frac{p_{i+1,j}-p_{i-1,j}}{2\Delta\xi},\quad \frac{\partial p}{\partial \eta}=\frac{p_{i,j+1}-p_{i,j-1}}{2\Delta\eta}\quad \text{for points adjacent to boundary.}$$

The second-order backward schemes for continuity equations are:

$$\frac{\partial \phi}{\partial \xi}=\frac{3\phi_{i,j}-4\phi_{i-1,j}+\phi_{i-2,j}}{2\Delta\xi},\quad \frac{\partial \phi}{\partial \eta}=\frac{3\phi_{i,j}-4\phi_{i,j-1}+\phi_{i,j-2}}{2\Delta\eta}\quad \text{for inner points}$$

$$\frac{\partial \phi}{\partial \xi}=\frac{\phi_{i+1,j}-\phi_{i-1,j}}{2\Delta\xi},\quad \frac{\partial \phi}{\partial \eta}=\frac{\phi_{i,j+1}-\phi_{i,j-1}}{2\Delta\eta}\quad \text{for points adjacent to boundary.}$$

The two momentum equations are coupled and solved by block TDMA (TriDiagonal Matric Algorithm) sweeping in ξ- and η-directions. From the discretized momentum equations, the following relations are derived:

$$\delta u_{\xi\, i,j} \approx b_{i,j}\delta p_{i,j}+b_{i,j+1}\delta p_{i,j+1}+b_{i+1,j}\delta p_{i+1,j}+b_{i+1,j+1}\delta p_{i+1,j+1} \tag{11a}$$

$$\delta u_{\eta\, i,j} \approx a_{i,j}\delta p_{i,j}+a_{i,j+1}\delta p_{i,j+1}+a_{i+1,j}\delta p_{i+1,j}+a_{i+1,j+1}\delta p_{i+1,j+1} \tag{11b}$$

The pressure correction equation is obtained in the same way as the SIMPLE algorithm of Patankar[14]. Substituting equation (11) into the differenced continuity equations, the pressure correction equation is obtained as:

$$\begin{aligned} d_{i,j}\delta p_{i,j}+d_{i+1,j}\delta p_{i+1,j}+d_{i-1,j}\delta p_{i-1,j}+d_{i-1,j+1}\delta p_{i-1,j+1}+d_{i,j+1}\delta p_{i,j+1} \\ +d_{i,j-1}\delta p_{i,j-1}+d_{i+1,j-1}\delta p_{i+1,j-1}=-R_c \end{aligned} \tag{12}$$

Equation (12) is solved by TDMA sweeping alternatively in ξ- and η-directions. The iteration continues until the maximum residual of each equation is reduced to 0.01. Through numerical experimentations, the under-relaxation factor for updating the velocity and pressure fields is optimally obtained as α_p = 0.2-0.4 rather than 0.75 as in the standard SIMPLE method[15].

The present work is concerned only with the initial stages of the impulsively started flow over a square cylinder. The numerical solution of the impulsively started flow over the square cylinder is an initial boundary value problem. Besides the boundary conditions specified earlier, the velocities and pressure must be known at the initial time in order to carry out the numerical solution. The solution sequence for each flow condition is thus given by:

(1) At time $t = 0$, the velocities in the whole of the solution domain are given their values at the inlet section (hence, the term impulsively started flow). The initial pressure field is set to a reference value of zero.

(2) For $t > 0$, the ξ- and η-momentum equations are solved by block TDMA code. The residuals of these two equations are obtained.

(3) The residual of the continuity equations is calculated and used to solve the pressure correction equation.

(4) The velocity and pressure fields are updated by using the corrected pressure field.

(5) The maximum residual of the overall governing equations is obtained. If this maximum residual is greater than 0.01, the computation will return to step (2).

(6) At convergence, the streamline function is calculated from the velocity fields. The information for pressure coefficients, drag coefficient, etc. are obtained from the pressure field. The wake length is estimated from the above solutions.

In the above computational procedures, the velocities at the corners of the square cylinder are undefined. Hence, the conditions in these areas are treated separately. Here the multi-domain iterative procedure is introduced with the whole computational domain being divided into four subdomains and the sharp corners are located at the boundary of each of the subdomains. This method simplifies the definition of boundary conditions at the sharp corners. They are now treated as a solid boundary of one of the subdomains when numerical iterations of the entire solution domain are obtained.

RESULTS AND DISCUSSIONS

The numerical results obtained for flow past a square cylinder at Re = 25, 50, 250, 500 and 1,000 are presented here for study of the early stages of symmetrical wake flow developments. Computations of the symmetrical flow past the square cylinder were obtained up to a dimensionless time of $t = 8$. For the $t > 8$, the flow structures do not change significantly. The calculated results compared very well with the available numerical results reported by others. For example, the drag coefficients of configuration Number 4 of Davis and Moore[1] were similar to that presented in Figure 11 and the pressure contours of Lisa and Balasubramaniam[4] are similar to Figure 8.

The boundary conditions and the finite difference mesh used in the present study are shown in Figures 1 and 2 respectively. Following a series of initial numerical experimentations, the location of the square cylinder in the solution domain is chosen optimally at a distance forward of the centre of the computational domain. Significant flow developments are noted to occur in the wake flow and the upper and lower flow separation regions. The dimensions A, B, C, D, E, F as shown in Figure 1 are chosen as: $A = 7d$, $C = 7d$, $D = 4.5d$, $F = 14.5d$, $B = E = d$, where d is the dimension of a side of the square cylinder.

Figures 3-7 show the evolution with time of the impulsively started streamline flow structure over the square cylinder for Re = 25, 50, 250, 500 and 1,000 respectively. Immediately after the start of the flow, the flow is irrotational everywhere (type I main-flow). But as the flow moves

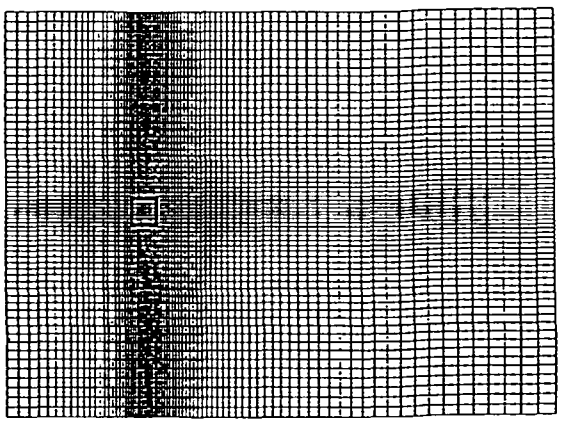

Figure 2 Finite difference mesh

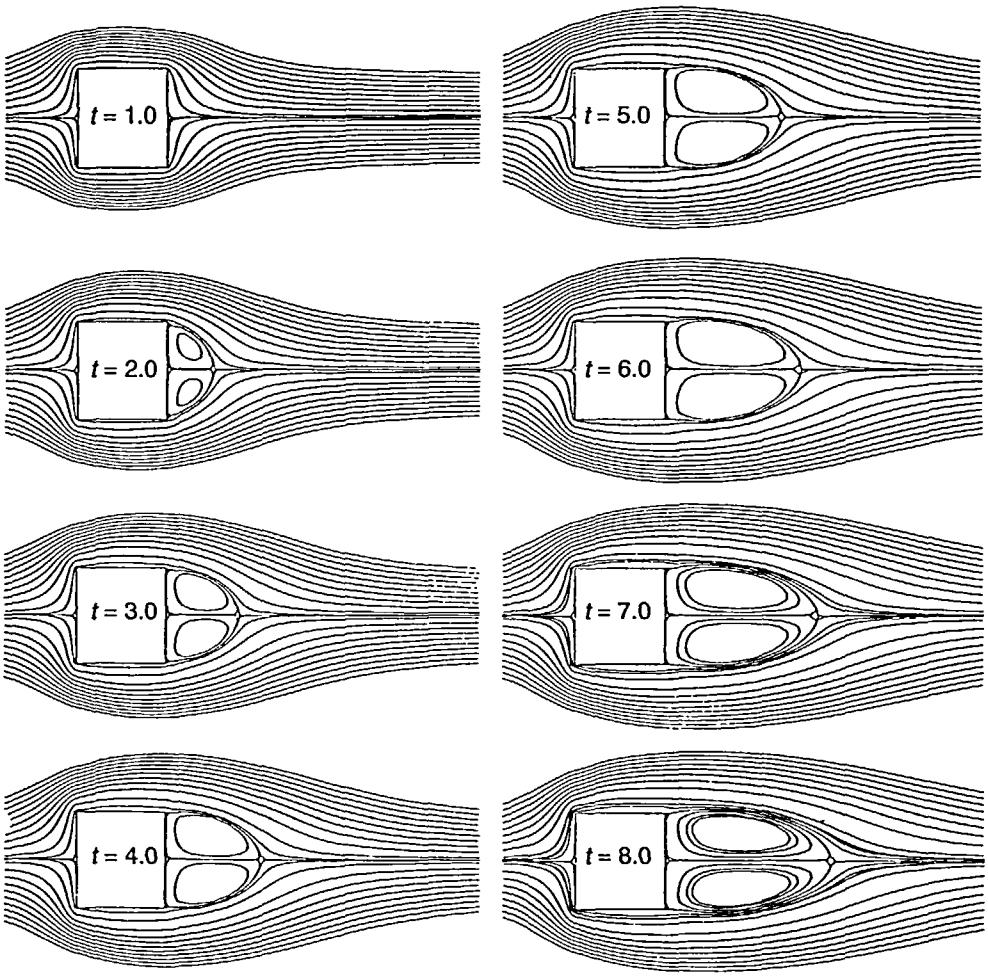

Figure 3 Instantaneous streamline pattern for Re = 25 at various times

over the square cylinder, vorticity is generated at the solid surface and transported to the region of the rear stagnation point, inducing a reversal flow. This reverse flow in time grows into a symmetrical standing zone of recirculation at the aft end of the cylinder (type II mainflow). Flow separation from the leading edges of the square cylinder also develops as time advances (type III main-flow). Above a critical Reynolds number Re_{crit}, and after a critical period of time (t^*) which is shorter as the Reynolds numbers become greater, the separated flows from the leading edges of the square cylinder merge with the swelling recirculation wake flow region at the aft end of the cylinder. This creates a complex recirculatory flow pattern (type IV main-flow) with possible tertiary recirculations at the meeting points of the type II and type III separated flows. However, the present investigation is limited to cases where the recirculation zones in which eddies develop remain symmetrical and stably attached to the square cylinder.

A simple qualitative examination of the developing streamline contours shows that the time development of the flow differs when Re is increasing. With regards to the Reynolds number, it is possible to distinguish three categories of flow time evolutions which correspond roughly to

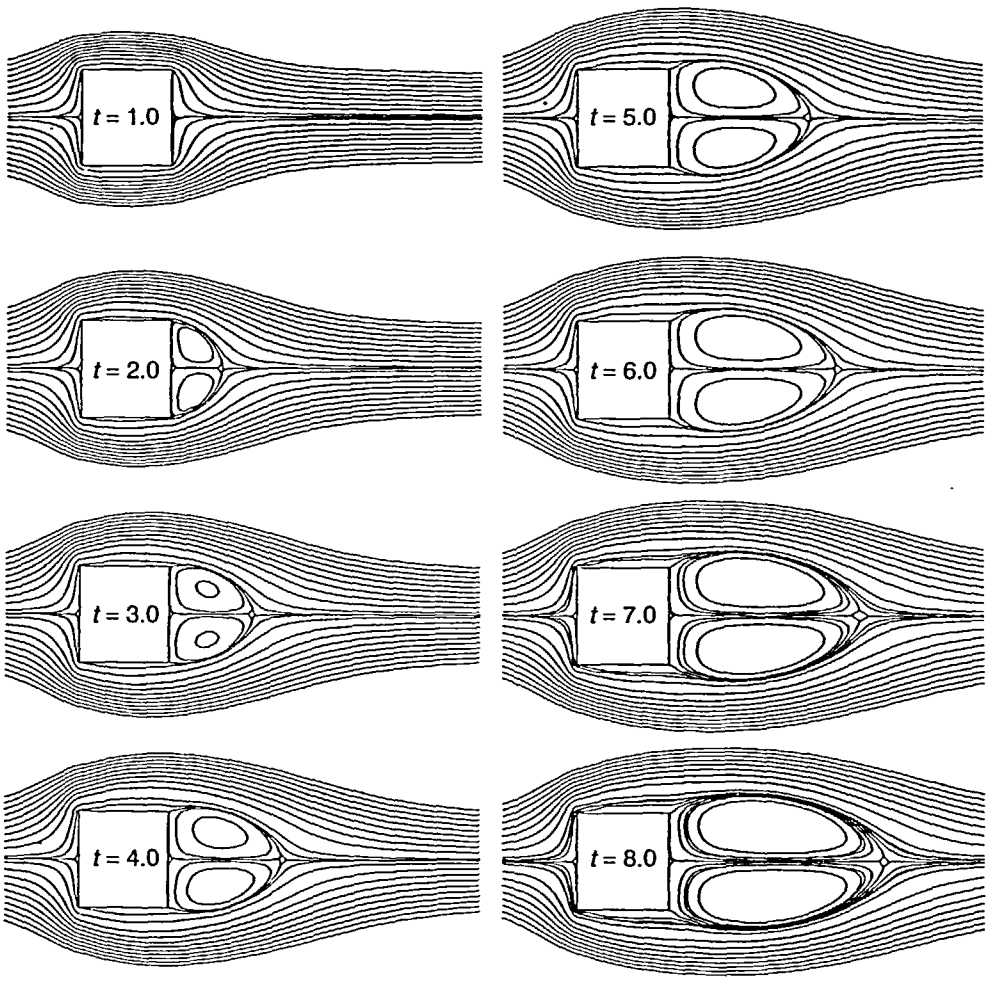

Figure 4 Instantaneous streamline pattern for Re = 50 at various times

small, moderate and high Reynolds numbers where the flow remains symmetrical and attached to the square cylinder:

$$Re < Re_1, \quad Re_1 < Re < Re_2 \quad \text{and} \quad Re > Re_2$$

The exact limiting values of Re_1 and Re_2 cannot be determined by this qualitative investigation; they will be classified subsequently by means of the numerical presentations of the streamline contours on the main characteristics of the flow. However, for the sake of illustration, it can be said that the values of Re_1 and Re_2 have been found to be approximately 25 and 250.

Time evolution at low Reynolds numbers: $Re < Re_1$

If the value of Re remain below a certain limiting value of Re_1 and the flow time is small ($t < 1.0$), the flow develops with time without visible flow separation and reattachment (type I main-flow). After a short lapse of time, the flow separates first from the rear surface of the square (type II main-flow) and forms aft end symmetrical eddies within a recirculating zone (sub-flow (a)). This unique recirculating zone consist typically of the two symmetrical eddies. For Re > 25 these twin

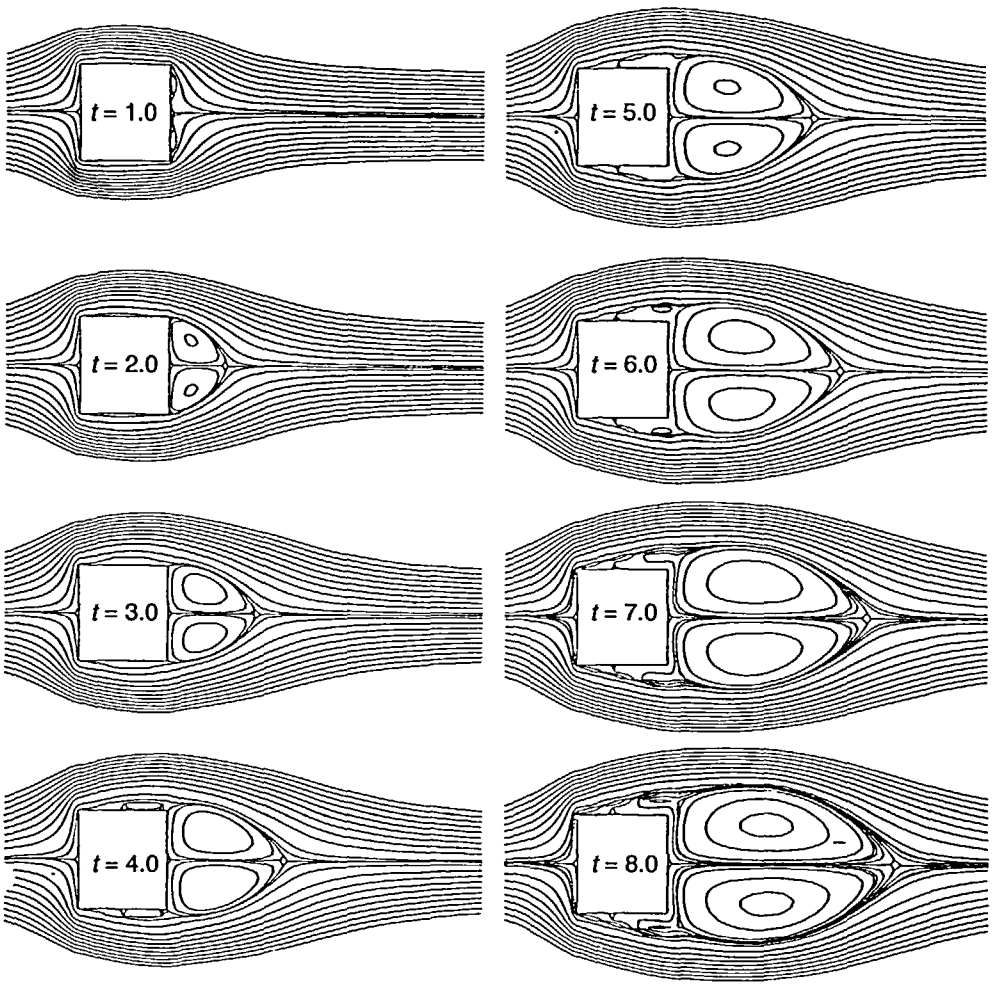

Figure 5 Instantaneous streamline pattern for Re = 250 at various times

eddies occur as soon as $t > 1.5$. The length and the width of the recirculation region increase as flow time advances.

Time evolution at moderate Reynolds numbers: $Re_1 < Re < Re_2$

As the Reynolds number is increased, the domains of the recirculating zone increase rapidly. Typical of this category of flow, recirculatory flow phenomena begin to appear during the flow development. First, near the sharp corners at the rear surface of the square cylinder, the fluid particles passing through this region deviate from the cylinder, causing a separation region in the streamline pattern. The recirculation region of the close wake is established. As flow time progresses, the streamlines separating from the leading edges of the upper and lower surfaces of the square cylinder (type III main-flow) merge with the growing recirculation region at the aft end of the cylinder. This results in a complex recirculatory flow pattern (type IV main-flow) with tertiary recirculations (sub-flow (c)) near the meeting points between the type II and type III flows. The complexity of the flow pattern depends on the Reynolds number.

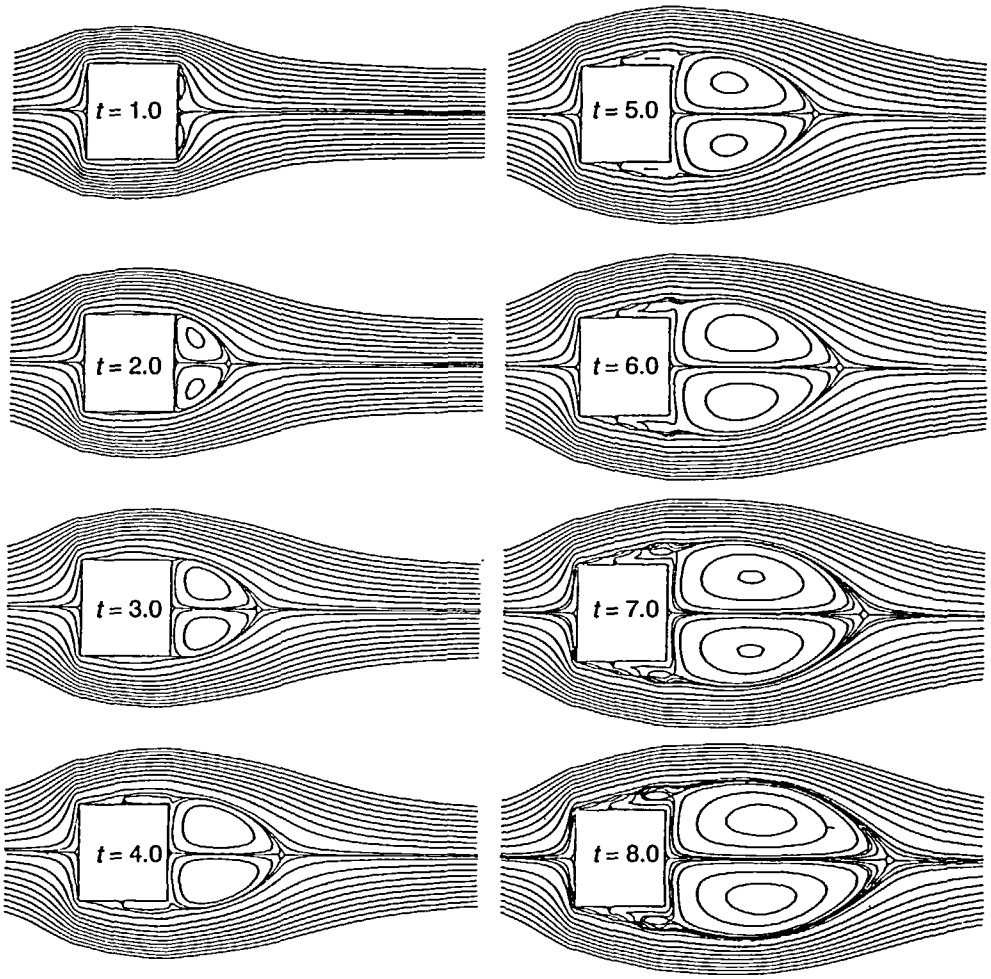

Figure 6 Instantaneous streamline pattern for Re = 500 at various times

For Re = 50, Figure 4 shows that at $t < 1.0$, there is no observable flow separation over the leading edges of the square cylinder. For $t > 1.0$, flow separations begin at the trailing edges of the square cylinder. The twin eddies can be seen issuing from the rear stagnation point of the square cylinder. For $t > 2.0$, the separated flow region grows in size and development of the symmetrical eddies can be seen through the corresponding streamline pattern behind the square cylinder.

For Re = 150, the twin eddies appears for $t > 1.0$ nearer to the rear corners rather than at the centre of the aft surface of the square cylinder. At $t = 2.0$, the streamlines separate at the leading corners of the square cylinder forming recirculatory flow regions at the upper and lower surfaces of the square cylinder. As time advances, these separated secondary flows move towards the rear end and join up with the recirculating flow in the wake region. A tertiary sub-flow region was identified.

Time evolution at high Reynolds numbers: Re > Re_2

Beyond the limiting value of Re_2, two different sorts of phenomena occur and complicate the time development of the flow. As seen from Figures 5, 6 and 7 after a certain lapse of time following

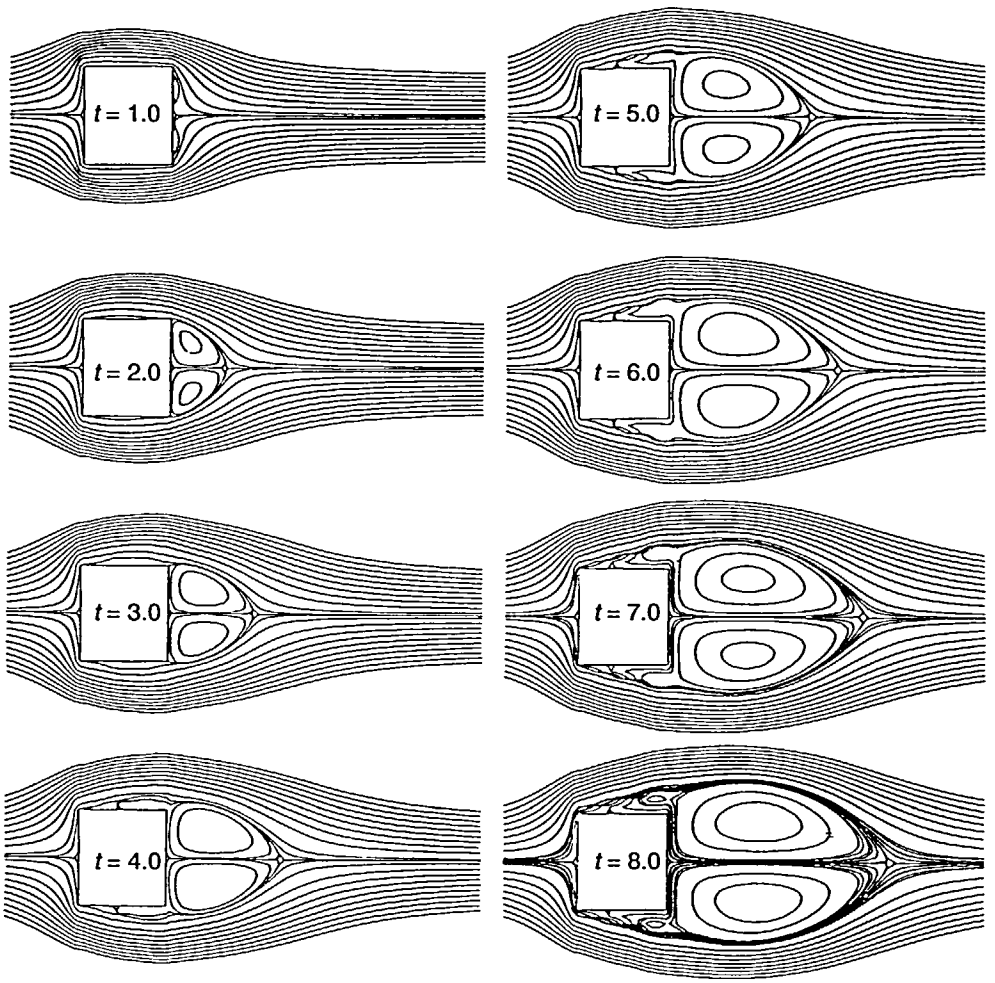

Figure 7 Instantaneous streamline pattern for Re = 1,000 at various times

the impulsively started flow over the square cylinder, the upper and lower surface shear layers begin to merge with the main recirculating zone at the aft end of the square cylinder, thus creating disturbances (sub-flow (c)) at the point of merging.

For Re = 250, 500 and 1,000, the sizes of the twin eddies at $t > 5$ time level are observed to be almost similar for these flows. However, the sizes of the separated shear layer at the upper and lower surfaces of the square cylinders are larger for higher Reynolds numbers at the corresponding time level. Thus, for a corresponding time level, the higher the Reynolds numbers, the larger will be the combined recirculatory flow region and the more obvious the tertiary recirculatory flow regime.

It should be pointed out here that for larger values of t, if an external disturbance is introduced, this will lead to vortex shedding. The flow solution may then bifurcate between symmetrical wake and Karman wake. It is also possible that the symmetrical wake at higher Reynolds numbers bifurcates between a steady state configuration and oscillating configuration or a periodic one of a different nature. These are not within the present scope of study.

Evolution of the flow characteristics in the sub-flow regions

Figures 3-7 also show the time evolution of the shape and structure of the various types of sub-flow (a) (b) and (c) for different values of the Reynolds number. The recirculation eddies at the aft end of the cylinder (sub-flow (a)) rotate in the same directions as the eddies at the upper and lower surfaces of the square cylinder (sub-flow (b)). The flow separation shear layers and the main recirculation zone grow in size with both time and as the Reynolds number increases.

For Re = 25, Figure 3 shows typically the time development of the sub-flow (a). It starts from the rear cylinder surface without presenting any variation in its concavities and remains smooth until its downstream extremities. It can be seen that in the earlier stage of the flow development the point of reattachment moves very quickly downstream. But from $t > 4.0$ the evolution becomes slow. At this value of Re, the maximum width of sub-flow (a) remains smaller than, or at most equal to, the width of the square cylinder.

For Re = 50, the outlines of the sub-flow (a) follow closely that for Re = 25 for $t < 4.0$. The width of the wake remains smaller than the width of the square cylinder. But for $t > 4.0$, the width of the wake becomes slightly larger than the width of the square cylinder.

For Re = 250, 500 and 1,000, the width of the wake of sub-flow (a) becomes clearly larger than the side of the square cylinder for $t > 3.0$. The separated flows (sub-flow (b)) develop from the leading edges of the square cylinder begin to merge with the recirculation zone in the wake region. For $t > 6.0$, the size of the recirculation zone, however, remains fairly similar for Re = 250, 500 or 1,000.

In general, the above study shows that for Reynolds numbers greater than a critical value and after a certain time period, separated flows from the leading edges of the square cylinder merge with the growing main recirculating zone aft of the cylinder. This creates a complex tertiary flow (sub-flow (c)) between the two merging recirculatory flows.

Evolution of other characteristics

Having made a comprehensive study by analysing the characteristics of the main recirculatory flow regions, we now consider the other derived characteristics of the flow, viz. the flow field pressure contours, the surface pressure coefficient, the wake length and the drag coefficient.

Figure 8 shows the pressure contours at $t = 8$ for the various range of Reynolds numbers considered here. For all the Reynolds numbers considered here, the pressure distributions in the fluid flow domain are generally symmetrical in nature. The development of the symmetrical eddies at the aft end of the cylinders can be observed from the changes of the pressure contours in the trailing wake region. For Re < 50, the recirculation pattern aft of the cylinder is small. For Re > 250, the pressure contours show a more complicated pattern than that of the lower Reynolds numbers of Re = 25 and 50. At Re = 250, the secondary recirculation region at the upper and lower surfaces of the cylinder can be seen merging with the wake region aft of the cylinder forming a single tertiary recirculating flow region between the separated flow from the leading edge and the recirculation region at the aft end of the cylinder. These pressure contours are also very similar to the pressure contours obtained by Lisa and Balasubramaniam[4].

Figure 9 presents the distribution of the pressure coefficients along the surfaces of the square cylinder and its variation with respect to time. The surface pressure distributions are obtained from the pressure contours described in Figure 8. Surface pressure coefficient is defined here as $Cp = p - p_\infty / \frac{1}{2} \rho u_\infty^2$. Figure 9 shows that the distributions of the surface pressure do not change significantly once the streamline flow field is established. The numbers 1, 2, 3 and 4 as shown on the x-axis of Figure 9 represent the four sharp corners of the square section as shown in Figure 1. It is observed that the surface pressure coefficients vary from a maximum positive value near the frontal stagnation point to a minimum (negative) value near the aft end of the two frontal sharp corners. The surface pressure coefficients tend rapidly towards a stationary value when the flow field is established as time advances.

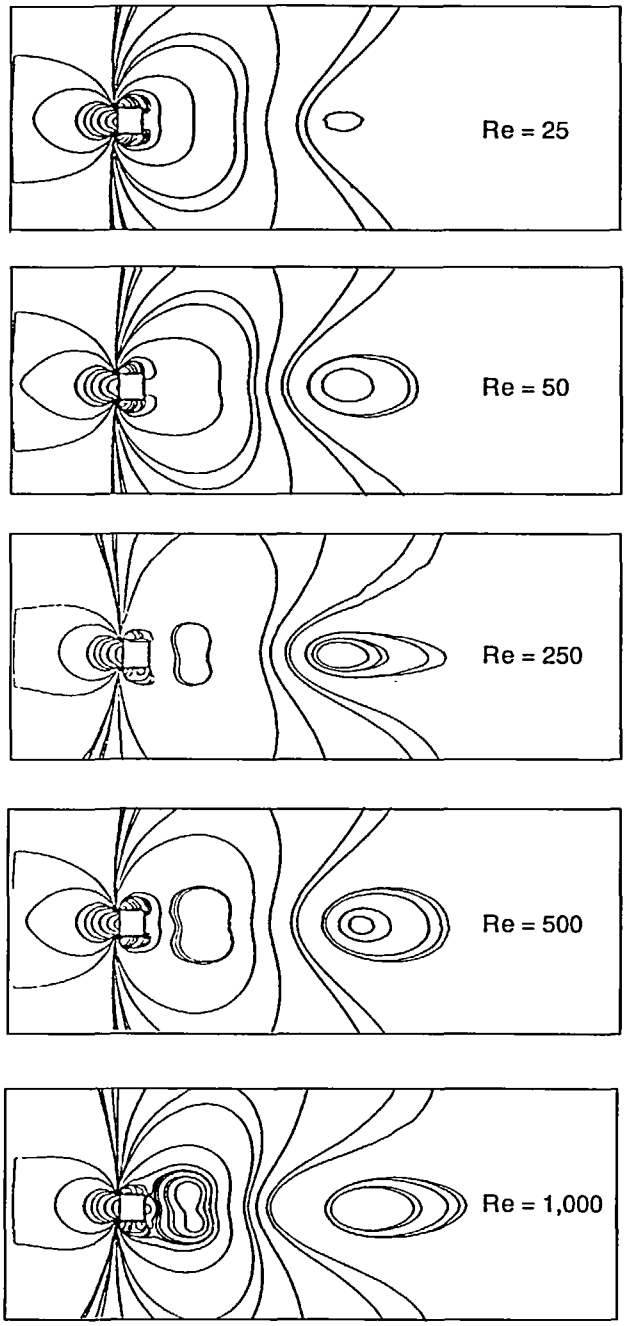

Figure 8 Pressure contours at $t = 8$ for different Reynolds numbers

The growth of the wake length with time for the various Reynolds numbers considered here is shown in Figure 10. The wake length is defined here as the distance between the centre of the rear surface of the square cylinder with respect to the downstream reattachment point (or stagnation

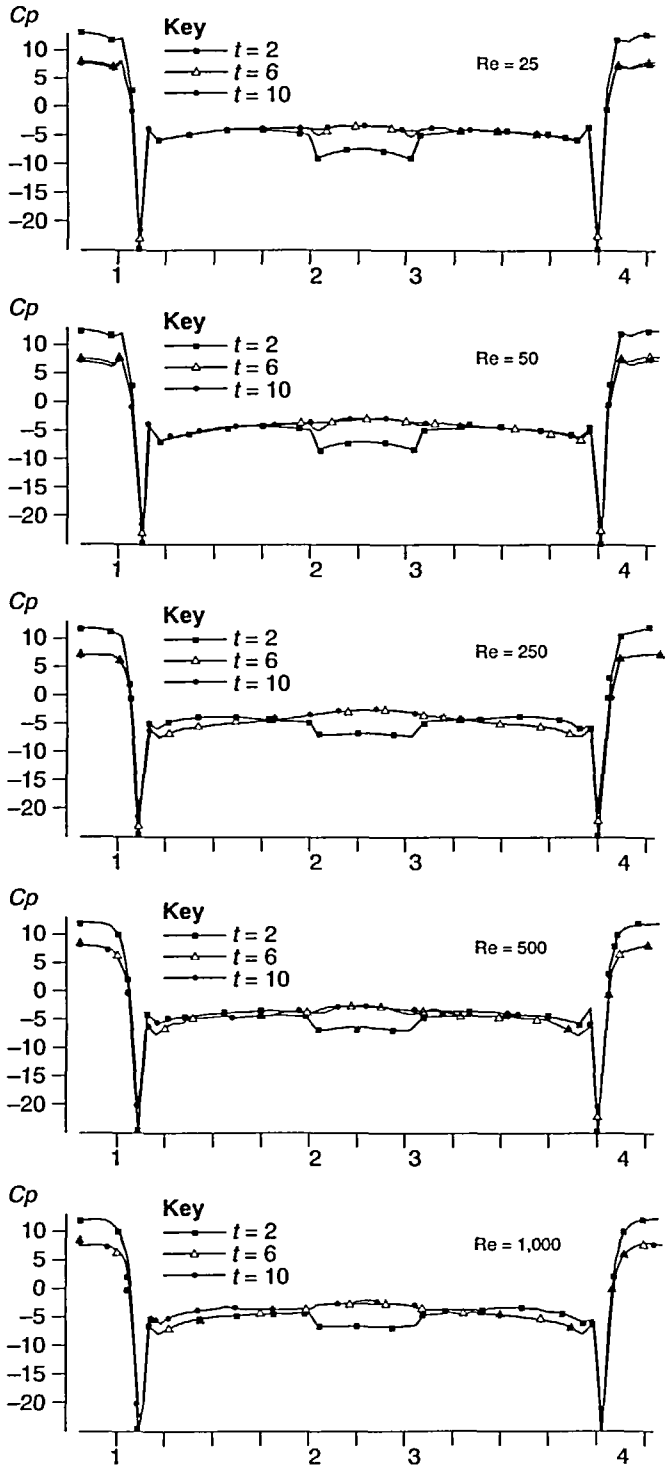

Figure 9 Time variation of surface pressure coefficient at different Reynolds numbers

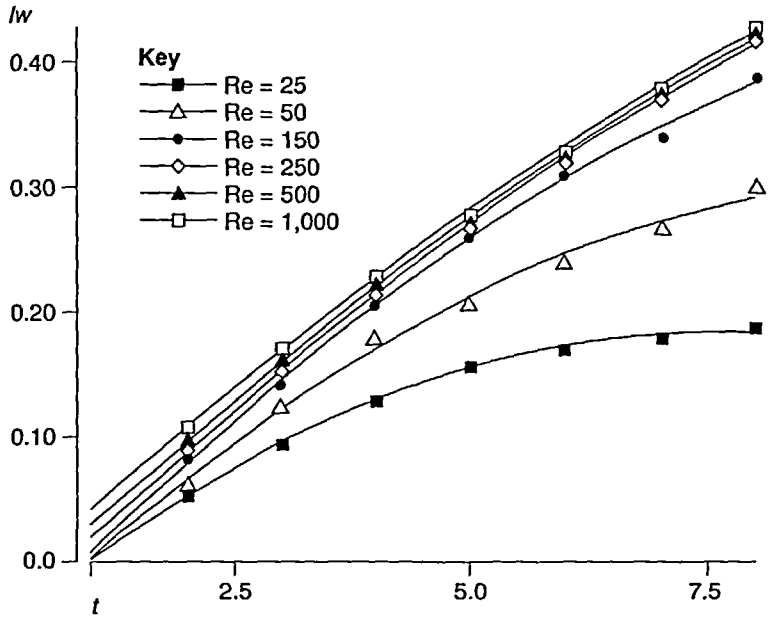

Figure 10 Time variation of wake length (*lw*) for various Re

point where $u = v = 0.0$) along the symmetrical axis of the square cylinder. The rate of increase of the wake length depends on the approaching flow Reynolds numbers. For Re = 25 and 50, the wake lengths behind the cylinder increase in a parabolic manner. For Re = 250, 500 and 1,000, the initial wake lengths increase almost linearly with time. For a fixed time level, the wake lengths for higher Re flows are longer, but generally approach some steady values as time advances.

Figure 11 shows the time evolution of the drag coefficient (Cd) for different Reynolds numbers. The Cd results were obtained from the surface pressure distributions as shown in Figure 9. For Re = 25 and 50, the drag coefficient decreases rapidly during the initial stages of the flow development and latter exhibits a more gradual change towards the steady value. For Re = 250, 500 and 1,000, the drag coefficients also decrease rapidly during the early stages of the flow development, initiating at lower values of Cd. The higher the Reynolds number, the lower is the initiating value of the drag coefficient. However, for Re > 250, the rate of decrease of the drag coefficients as time advances is similar. For 250 < Re < 1,000, there is no significant different for the Cd curves obtained here. The Cd value varies from 1.9 to 2.25. This is consistent with the Cd data reported in the literature for square cylinders. A comparison of drag coefficients obtained here with the data obtained by Davis and Moore[1] for a "configure 4-square cylinder" at Re = 1,000 with respect to the advancement of time shows same results.

CONCLUSIONS

Early stages of an impulsively started laminar flow around a square cylinder for 0 < Re < 1,000 are studied numerically. The computed results show that the characteristics of developing flow recirculation, flow separation and regimes caused by merging of flows are strongly dependent on the approaching Reynolds number. At any flow time level, the Reynolds number determines the flow characteristics. Four main flow regimes have been differentiated according to whether:

(1) the flow is attached predominantly onto all the surfaces of the square cylinder (type I);

(2) flow recirculation develops at the aft end of the cylinder surface (type II);

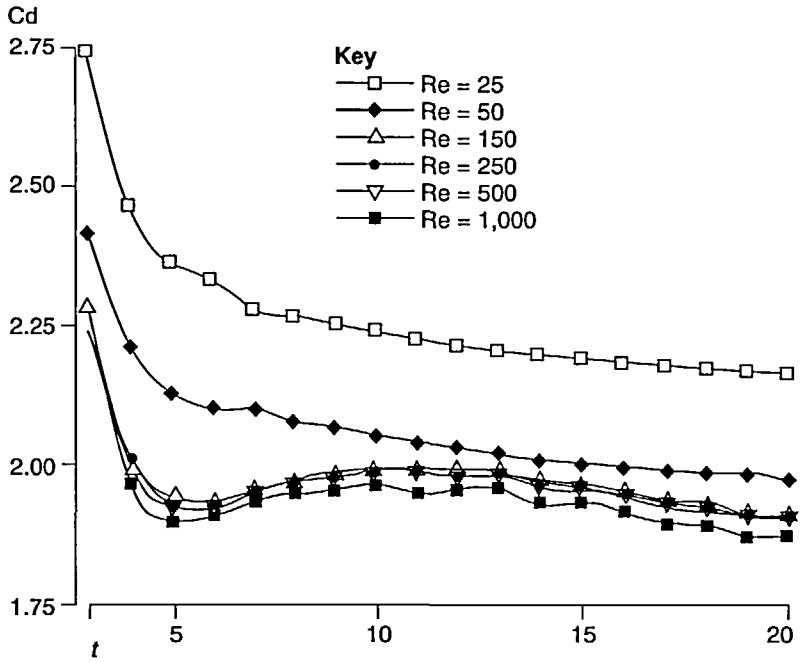

Figure 11 Time variation of drag coefficient (Cd) for various Re

(3) there is significant flow separation from the leading edges of the square cylinder (type III);
(4) there is growing of the aft end recirculation zone and the merging with the separating flow zone from the leading edges, forming a complex tertiary flow phenomenon at the boundary of the two main mixing zones (type IV).

Within the Type I-IV main flow characteristics, three significant sub-flow regimes were also identified. Sub-flow (a) examines the growing and development of the symmetrical eddies aft of the cylinder surface; sub-flow (b) looks at the spreading of the separating shear layer from the leading edges of the square cylinder; and sub-flow (c) analyses the complex disturbed flow regime near the meeting point between the developing type II and type III flows.

For $Re < 25$, the initial flow develops with time without visible flow separation (type I). After a short lapse of time, the flow separates predominantly from the rear surface of the square and forms symmetrical eddies within a recirculating zone about the rear axis of the cylinder (type II). For $25 < Re < 250$, a significant secondary phenomenon was observed early, viz. the development of a flow separation on the upper and lower surfaces of the square cylinder (type III). For $Re > 250$, the merging of the separation flow (type II) from the upper and lower cylinder with the recirculation zone of the wake region (type II) forming type IV flow was observed. For a given Re, once type II and type III recirculatory flows merge, the overall recirculation flow of type IV flow usually remains fairly constant with the advancement of time.

The time evolution of the various characteristics of the sub-flow regions occur during different phases of the main flow developments. Initially, the primary recirculatory region aft of the cylinder (sub-flow (a)) grows with the width of the wake less than the width of the square cylinder. As time advances, sub-flow (a) grows wider than the width of the square cylinder, and eventually merges with the elongated upper and lower separated surface shear layers (sub-flow (b)) from the leading edges of the square cylinder. When sub-flows (a) and (b) merge, complex tertiary sub-flow (c) region develops at the merging point. At this stage, the recirculating zone at the aft end of

the cylinder grows wider than the width of the square cylinder. The length of the separating shear layer from the leading edges grows longer than the length of the square cylinder.

Individualization of a rapid vortex source during the very early phase of the flow evolution was also observed. This gives rise to the main eddy which occurs near the aft end of the cylinder. Subsequently, a rear stagnation point is then formed away from the aft surface of the square cylinder. This downstream stagnation point moves rapidly downstream as the Re increases and is a measure of the wake length for the flow development.

ACKNOWLEDGEMENTS

The authors gratefully acknowledge the financial assistance of a research grant RP890633 from the National University of Singapore. The assistance of Dr S.H. Winoto during the course of this work is also gratefully acknowledged.

REFERENCES

1 Davis, R.W. and Moore, E.F., A numerical study of vortex shedding from rectangles, *J. Fluid Mech*, **116**, 475-506 (1982)
2 Nagano, S., A numerical analysis of two-dimensional flow past a rectangular prism by a discrete cortex model, *Computers and Fluids*, **10**, 243-259 (1982)
3 Fernando, M.S.U.K. and Modi, V.J., A numerical analysis of unsteady flow past bluff bodies, *Computational Mechanics*, **6**, 11-34, (1990)
4 Lisa, M.L. and Balasubramaniam, R., Numerical analysis on strouhal frequencies in vortex shedding over square cylinders with surface suction and blowing, *Int. J. Num. Meth. Heat Fluid Flow*, **3**, 357-375 (1993)
5 Kim, S .W. and Benson, T.J., Comparison of the SMAC, PICO and ITERATIVE TIME-ADVANCING schemes for unsteady flows, **21**, 435-454 (1992)
6 Bearman, P.W. and Trueman, D.M., An investigation of the flow around rectangular cylinders, *Aeronautic Quarterly*, **23**, 229-237 (1972)
7 Coutanceau, M. and Bouard, R., Experimental determination of the main features of the viscous hydrodynamic field in the wake of a circular cylinder in a uniform stream, *J.Fluid Mech*, **79**, 231 (1977)
8 Bouard, R. and Coutanceau, M., The early stage of development of the wake behind an impulsively started cylinder for $40 < Re < 10^4$, *J. Fluid Mechanics*, **101**, Part 3, 583-607 (1980)
9 Gerrard, J.H., The mechanics of the formation region of vortices behind bluff bodies, *Journal of Fluid Mechanics*, **25**, 401 (1966)
10 Gerrard, J.H., The wakes of cylindrical bluff bodies at low Reynolds number, *Phil. Trans. Roy. Soc. A*, **288**, 29 (1978)
11 Okajima, A., Strouhal numbers of rectangular cylinders, *J. Fluid. Mech*, **123**, 379-398 (1982)
12 Okajima, A. and Kitajima, K., Numerical study on wake patterns and aerodynamic forces of an oscillating cylinder with a circular and rectangular cross-section, *Journal of Wind Engineering and Industrial Aerodynamics*, **50**, 39-48 (1993)
13 Kyoji, K. and Yoshifumi, Y., Observation of the flow around a circular cylinder and a trapezoidal cylinder in a circular pipe by a dye-injection method, *11th Australasian Fluid Mech. Conference* (14-18 December 1992)
14 Patankar, S.V., *Numerical Heat Transfer and Fluid Flow*, Hemisphere, Washington, DC (1980).
15 Doormal, J.P.V. and Raithby, G.D., Enhancements of the SIMPLE method for predicting incompressible fluid flows, *Numerical Heat Transfer*, **7**, 147-163 (1984)